2012

Color texture analysis based on fractal descriptors

PATTERN RECOGNITION, OXFORD, v. 45, n. 5, supl. 1, Part 1, pp. 1984-1992, MAY, 2012
http://www.producao.usp.br/handle/BDPI/32552

Pattern Recognition 45 (2012) 1984–1992

Contents lists available at SciVerse ScienceDirect

Pattern Recognition

journal homepage: www.elsevier.com/locate/pr

Color texture analysis based on fractal descriptors

André Ricardo Backes [a,*], Dalcimar Casanova [b,1], Odemir Martinez Bruno [b,1]

[a] Faculdade de Computação, Universidade Federal de Uberlândia, Av. João Naves de Ávila, 2121, 38408-100, Uberlândia, MG, Brazil
[b] Instituto de Física de São Carlos (IFSC), Universidade de São Paulo, Av. Trabalhador São Carlense, 400 13560-970 São Carlos, SP, Brazil

ARTICLE INFO

Article history:
Received 11 May 2011
Received in revised form
29 September 2011
Accepted 15 November 2011
Available online 25 November 2011

Keywords:
Color texture analysis
Fractal dimension
Complexity
Feature extraction
Classification

ABSTRACT

Color texture classification is an important step in image segmentation and recognition. The color information is especially important in textures of natural scenes, such as leaves surfaces, terrains models, etc. In this paper, we propose a novel approach based on the fractal dimension for color texture analysis. The proposed approach investigates the complexity in R, G and B color channels to characterize a texture sample. We also propose to study all channels in combination, taking into consideration the correlations between them. Both these approaches use the volumetric version of the Bouligand–Minkowski Fractal Dimension method. The results show a advantage of the proposed method over other color texture analysis methods.

1. Introduction

The identification of visual patterns has long been an area of computer vision with active research. Texture analysis can be very useful for experiments of image classification and identification. While the ability of a human to distinguish different textures is apparent, the automated description and recognition of these same patterns have proven to be quite complex.

Over the years, researchers have studied different texture analysis approaches. Many of these approaches represent the local behavior of the texture via statistical [1], structural [2] or spectral [3–5] properties of the image. Good surveys can be found in [5–11]. The conjecture presented in [12], where second-order probability distributions [6,13] are enough for human discrimination of two texture patterns, has motivated the use of statistical approaches. This conjecture showed not to hold strictly particularities when textures present some structure [14]. Structural approaches, then, attempt to describe a texture by rules, which govern the position of primitive elements, which make up the texture [15]. In addition, signal processing methods, such as Gabor filters [4,16,17], Fourier analysis [18] and Wavelet packets [19], were motivated by psychophysical researches, which have given evidences that the human brain does a frequency analysis of the image [20,21]. These approaches represent the texture as an image in a space whose coordinate system has an interpretation that is closely related to the characteristics of a texture (such as frequency or size).

However, these methods fail to distinguish many natural textures that show no periodic structure [22]. Natural textures may not present any detectable quasi-periodic structure. Instead, they exhibit random, but persistent, patterns that result in a cloud-like texture appearance. Examples of these *cloudy* textures are widely found on nature (pictures of clouds, smoke, leaves surfaces, terrain models, etc.).

Fractals offer an interesting alternative to these approaches. Due to its irregularities, most of the natural surfaces have non-integer dimension. Therefore, it seems plausible that the fractal model might also be applied successfully to analyze images. This reduces the classification problem to estimating the fractal dimension of the texture. Since the fractal feature is an inherent property of the region/surface/object, it can be considered a more reliable measure [23]. In fact, according with [24], the fractal dimension is a very useful metric for the analysis of the images with self-similar content, such as textures.

The fractal dimension (D) shows a strong correlation with human perception of surface roughness. Several methods have been developed to estimate D for image analysis. In [25], the fractal dimension is estimated using the Fourier power spectrum of the image's intensity surface modeled as fractal Brownian motion surface. In [26], Mandelbrot's idea of the ϵ-blanket method is adopted and extended for surface area calculation. The box-counting method, developed by [27], and its improved version, called differential box-counting (DBC) and developed by [28–30], have been used for several tasks of texture comparison and classification, and object characterization [31,32]. Subsequently, [33,34] have applied the

* Corresponding author. Tel.: +55 34 32394499.
E-mail addresses: arbackes@yahoo.com.br, backes@facom.ufu.br (A.R. Backes), dalcimar@gmail.com (D. Casanova), bruno@ifsc.usp.br (O.M. Bruno).
[1] Tel.: +55 16 3373 8728; fax: +55 16 3373 9879.

0031-3203/$ - see front matter © 2011 Elsevier Ltd. All rights reserved.
doi:10.1016/j.patcog.2011.11.009

multi-fractal theory for texture classification and segmentation, while [35,36] have adopted the method of Bouligand–Minkowski fractal dimension to estimate the complexity of images.

However, all these methods present the inconvenient of working only with gray-scale images. It has been proven that color information is quite useful in image analysis [37,38], in special on natural textures (leaves surfaces, terrain models, etc.). Therefore, a fractal dimension method for multi-spectral images (color images) is quite interesting. Recently, [24] presented a study with fractal dimension in color images. It was proposed a new method for generate color fractal images. Additionally he use the Voss algorithm to estimate the fractal dimension of these images. However, the use of the fractal dimension alone, as a unique feature describing the texture, is not suitable for classification problems with many classes. The work of [37] has adopted a fractal-based method for texture segmentation of color images (multi-spectral). This method is based on local pixel analysis for *only* segmentation applications. Thus, we propose an approach which is based on a global texture analysis for the classification of color textures, and not only segmentation. Our approach can perform the analysis of each color channel independently (as in the work of [37]), as also to study the relationship between color channels altogether, in a sort of multi-spectral approach, what we believe to be an interesting approach for image analysis.

This paper starts by presenting an overview of the fractal dimension and the details of our approach, the volumetric fractal dimension (Section 2). Section 3 presents the proposed signature that we use to characterize a texture pattern. The benefits of this approach are set out and its use in color texture is described in Section 4. An experiment is set to evaluate the performance of the proposed texture signature in the classification of different color texture sets (Section 5). Section 6 shows the results yielded by the proposed method, while in Section 8, the conclusions about the method are discussed.

2. Fractal dimension

In 1970s, Benoit Mandelbrot introduced the world to a new field of mathematics. Mandelbrot named this field of Fractal Geometry. He introduced a new class of sets called fractals: objects of great complexity which are generated from iteration of simple rules. These Fractals also presented a non-integer dimension, which is related to their complexity and space occupation [39,40].

The fractal dimension, D, is based on the concept of self-similarity, and it should be independent of the method chosen to its estimation. Unfortunately, different methods estimate different values for D, especially to characterize objects with limited self-similarity, such as texture images. One of the most accurate methods to estimate the fractal dimension of a shape image is the Bouligand–Minkowski method [41]. This method is based on the study of the influence area of the object contained in the image, and it is very sensitive to structural changes of the object.

Although its common use in shape analysis, the complexity of a texture image can be easily estimated by using the Bouligand–Minkowski method [36]. This is possible by mapping the entire texture image surface onto a 3D volume $S \in R^3$. Fig. 1 shows an example of this texture image surface. By dilating the surface mapped in S by a radius r, it is possible to estimate the Bouligand–Minkowski fractal dimension D as the (continuous) plot of $\log(V(r))$ versus $\log(r)$, where $V(r)$ is the influence volume computed through dilation of each point of the surface in S using a sphere of radius r

$$D = 3 - \lim_{r \to 0} \frac{\log V(r)}{\log (r)} \tag{1}$$

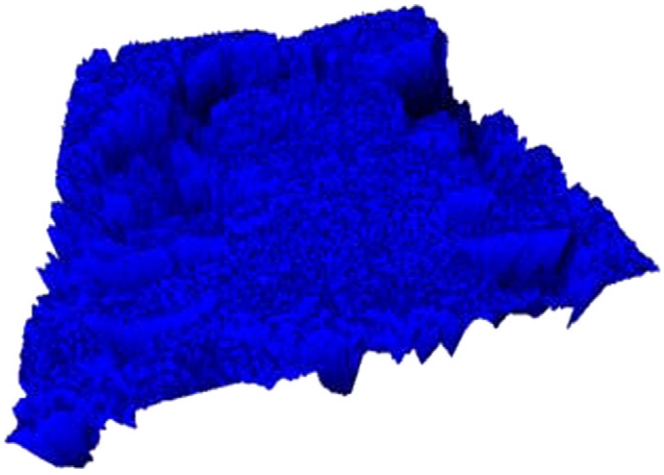

Fig. 1. Texture image surface before applying the Volumetric Bouligand–Minkowski fractal dimension [36].

with

$$V(r) = \{p \in R^3 \,|\, \exists p' \in S : |p - p'| \leq r\}. \tag{2}$$

As the influence area computed for shape analysis, the influence volume of a texture is also very sensitive to structural changes (spacial distribution), so even small changes in the texture behavior can be detected.

2.1. Surface mapping and dilation process

To compute the dilation of a surface is a time consuming task. One approach to optimize this task is to use the Euclidean Distance Transform (EDT). This transform computes a distance map for the 3D volume, where each voxel value represents the minimum distance from that voxel to the surface [42,43]. Let $I(x,y)$, $x=1 \ldots N$ and $y=1 \ldots M$, a pixel in an image I, where x and y are the Cartesian coordinates of the pixel $I(x,y)$, and $I(x,y)=g$, $g=0,\ldots,L$ is an integer value, which represents the intensity of light in that pixel.

From this image I and using a dilation radius r, we build a 3D volume $S(u,v,w) \in R^3$, with $u = 1,\ldots,N+2r$, $v = 1,\ldots,M+2r$, $w = 1,\ldots,L+2r$

$$\forall I(x,y), S(u,v,w) = \begin{cases} 0 & \text{if } (u,v,w) = (x+r, y+r, I(x,y)+1+r), \\ C & \text{otherwise.} \end{cases} \tag{3}$$

where C is the maximum value allowed for the dilation radius r in the volume S. This value is defined as

$$C = \sqrt{\left(\frac{N}{2}+r\right)^2 + \left(\frac{M}{2}+r\right)^2 + \left(\frac{L}{2}+r\right)^2}. \tag{4}$$

Fig. 2 shows an example of the image to 3D volume mapping process. Basically, for a $N \times M$ pixels image with L gray levels, it is necessary to build a 3D volume of size $(N+2r) \times (M+2r) \times (L+2r+1)$. In this example, we have a 4×4 pixels image with 3 gray levels (Fig. 2a). By considering a dilation radius $r=1$, we build a 3D volume of size $6 \times 6 \times 5$ (Fig. 2b). By applying Eq. (3), we associate to each voxel a value 0 or C, where 0 represents where the voxel coincides with the texture image surface I, and C represents a point in the volume space whose distance to the texture image surface is still unknown (C is just a numeric representation to an infinite distance).

We perform the dilation process by computing the minimum distance between each two voxels of the volume S, where one of these voxels is marked as background (i.e., $S(u,v,w)=C$) and the other represents the surface of the original texture image

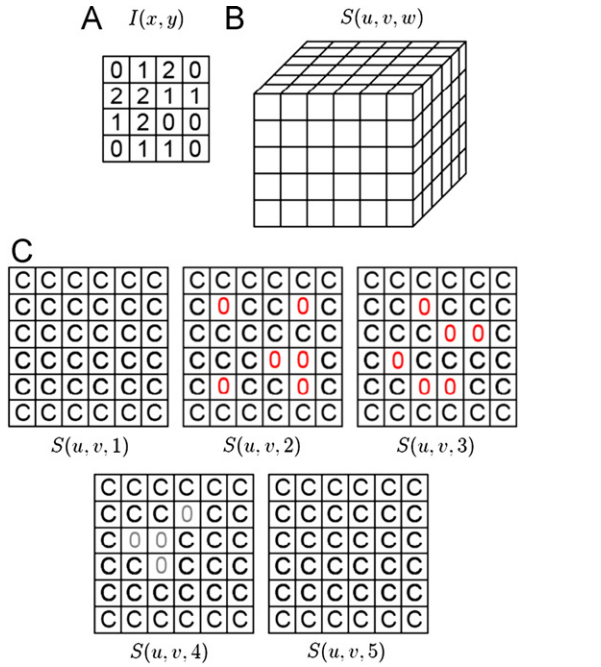

Fig. 2. Example of image to 3D volume mapping: (A) 4×4 pixels image with 3 gray levels; (B) 3D volume built using $r=1$; (C) voxel values of the 3D volume after applying Eq. (3).

(i.e., $S(u,v,w)=0$)

$$\forall S(u,v,w)=C, S(u,v,w)=\min d(u,v,w,u',v',w'), \tag{5}$$

where

$$d(u,v,w,u',v',w')=\sqrt{(u-u')^2+(v-v')^2+(w-w')^2} \tag{6}$$

and

$$S(u',v',w')=0. \tag{7}$$

After the dilation process is completed, it is necessary to compute the influence volume $V(r_i)$ for each radius value $r_i\le r$, where r is the maximum radius value. Be r_i a list of sorted radius values ranging from 0 to r, $r_i=\{0,1,\sqrt{2},\dots r\}$, where $r_i=\sqrt{x^2+y^2+z^2}$, $0\le x,y,z\le r$. We compute the volume $V(r_i)$ of the surface as the number of coordinates $S(u,v,w)$ whose distance from the surface is equal to r_i

$$V(r_i)=\sum_{u=1}^{N+2r}\sum_{v=1}^{M+2r}\sum_{w=1}^{L+2r}\delta(S(u,v,w),r_i), \tag{8}$$

where $\delta(a,b)$ is

$$\delta(a,b)=\begin{cases}1, & a\le b,\\ 0, & a>b.\end{cases} \tag{9}$$

From this point, the fractal dimension is estimated as the slope α of the (continuous) plot of $\log(V(r))$ versus $\log(r)$. This task is easily performed using a linear interpolation method, such as the linear least squares [44].

3. Fractal signature

The fractal dimension is a property of fractal objects related with the concept of self-similarity at infinite scales. However, images, as other real objects, have limited resolution and finite size. This makes their self-similarity to be limited to some scales. As a consequence, the complexity of the image changes according to the scale used in the visualization. This is noticed by studying the behavior of the log–log curve computed by the Bouligand–Minkowski method. This curve presents a richness of details that cannot be described by using a simple line regression as used in the classical fractal dimension estimation process.

Thus, we propose a feature vector which explores these curve details to perform a more accurate texture characterization. Initially, we compute the log–log curve using the Bouligand–Minkowski method for a dilation radius r. Then, we estimate a line which approximates this curve as $y=a*x+b$, where x and y are, respectively, the log of the radius r and the influence volume $V(r)$, a is the slope and b gives the y-intercept of the line. Note that, as defined in Section 2, $D=3-a$ is the estimated fractal dimension of the image.

This computed line is just an approximation of the real behavior of the log–log curve. There is an error between this line and the computed log–log curve. This occurs because each value of the log–log curve changes according to pixel position and color, both characteristics related to the image context and which cannot be described by a simple object as a line. Thus, the difference between line regression and the log–log curve at a given point is defined as the simple difference e_i

$$e_i=a\times\log r_i+b-\log V(r_i), \tag{10}$$

where $r_i\in[1,r]$ is a radius value which exists in the log–log curve and r is the dilation radius used to compute this curve. Texture characterization is performed by selecting a total of n equidistant radius values from the log–log curve to compose a feature vector $\psi(n)$

$$\psi(n)=[e_1,e_2,\dots,e_n]. \tag{11}$$

4. Image color information—a multi-spectral approach

Color information has proven to be quite useful for image analysis [37,38], especially when dealing with natural textures (leaves surfaces, terrains models, etc.).

According with [45] the color texture analysis can be roughly divided into two categories: methods that process color and texture information separately, and those that consider color and texture a joint phenomenon. For the second category we have the vectorial and marginal methods. The vectorial approach analyse the color channels presented in a texture altogether. It is a more recent approach and have many good papers (e.g. [46–48]). On the other hand, we have the older, but not less suitable, marginal approaches. This class of methods deals with color by analyzing each color channel independent of each other (e.g. [45]).

Our method can be adopted to belong to these two main approaches. For the marginal approach, we compute the descriptors for each color channel and combine them to compose a feature vector for that color texture. Thus, we achieve a $\varphi(n)$ feature vector, which consists of the fractal signatures $\psi_K(n)$ computed for each color channel K. For a *RGB* color texture, the following feature vector is obtained:

$$\varphi(n)=[\psi_R(n)\psi_G(n)\psi_B(n)]. \tag{12}$$

It is also possible to map each color channel present in the texture as a different surfaces in the R^3, thus building a vectorial method, that analyses the three channels in a single step (i.e., in a single 3D volume). Let $R(x,y)$, $G(x,y)$ and $B(x,y)$ be each color channel in a *RGB* color texture $I(x,y)$ and $S_R(u,v,w)$, $S_G(u,v,w)$, $S_B(u,v,w)$ their respective 3D volumes obtained using Eq. (3). These three volumes can easily be combined onto a single volume $S_{RGB}(u,v,w)$

$$S_{RGB}(u,v,w)=\begin{cases}0 & \text{if } S_R(u,v,w)=S_G(u,v,w)=S_B(u,v,w)=0,\\ C & \text{otherwise.}\end{cases} \tag{13}$$

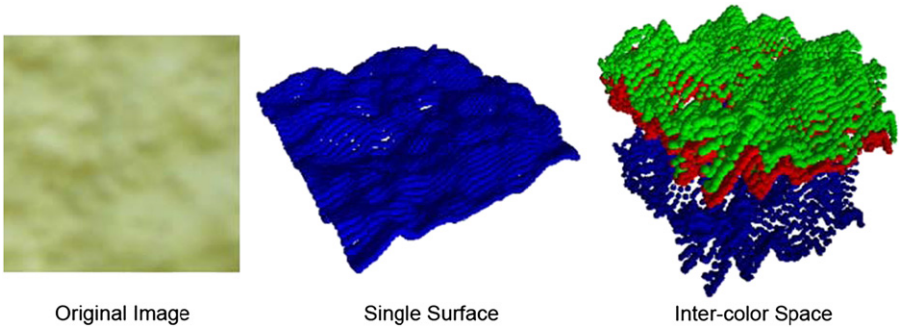

Fig. 3. Difference of surfaces generated by a gray-scale image and a color image (R, G and B components). (For interpretation of the references to color in this figure legend, the reader is referred to the web version of this article.)

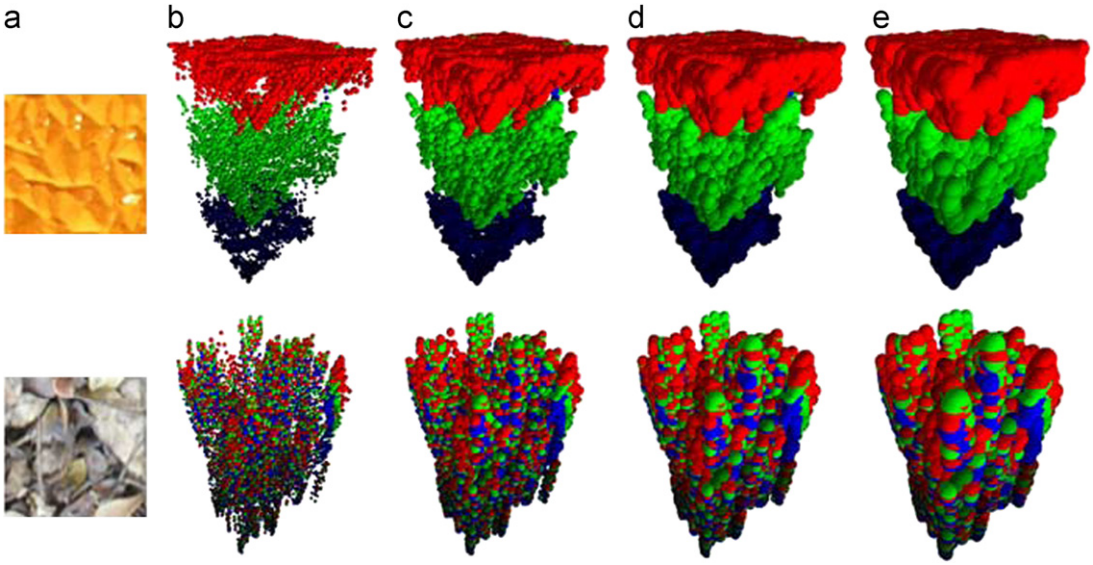

Fig. 4. Examples of color channel relationship during the dilation process for two color textures (first row, weak correlation; second row, strong correlation): (a) original texture; (b) $r=1$; (c) $r=2$; (d) $r=3$; (e) $r=4$. (For interpretation of the references to color in this figure legend, the reader is referred to the web version of this article.)

By considering the dilation process (described in Eq. (5)) over this new volume, it is possible to explore the relationship between the color channels of the texture pattern, instead of the characteristics of a single color channel. Thus, we yield a new signature $\psi_{RGB}(n)$, where *RGB* indicates that all color channels were dilated during the fractal dimension estimation process. This signature enables us to study all channels in combination, taking into consideration the correlations between them. Fig. 3 shows an example of all channel from a *RGB* color texture mapped as surfaces.

This approach considers that similar or equal intensities in different color channels represent a strong correlations between the surfaces, while different color intensities represent a weak correlation. The relationship between these surfaces changes when the dilation process occurs, and it modifies the resulting influence volume $V(r)$ by adding information about the distance between the surfaces. Surfaces which present a weak correlation can dilate their spheres freely for longer distances, and it produces a higher influence volume. Otherwise, a strong correlations between the channels causes one surface to obstruct the dilation process of another, thus resulting in a lower influence volume. Fig. 4 shows this process by dilating two surfaces over different r values. Therefore, this approach considers the concept of self-similarity and self-affinity between color channels.

It is important to remember that the dilatation process is affected by color and spacial distributions of pixels together. The color interaction is only part of the volume composition. Thus, the color information contributes with the method, but has no role alone.

5. Experiment

To evaluate the quality of our approach, we proposed an experiment using two color image databases. First database consists of texture images selected from VisTex [49]. A total of 640 samples grouped into 40 texture classes was considered. Each database entry class is a set of 16 texture samples of 128×128 pixels size, each one extracted from a particular texture pattern without overlapping. Fig. 5 shows examples of textures in the VisTex database.

Second database, called as USPTex, consists of a set of natural texture images acquired using a digital camera with 512×384 pixels resolution. Texture classes considered are typically found daily, such as beans, rice, tissues, road scenes, various types of vegetation, walls, clouds, soils, blacktop, and gravel. Each database entry class is a set of 12 texture samples of 128×128 pixels size, each one extracted from a particular material without overlapping. A total of 2160 samples grouped into 180 classes were considered. Fig. 6 shows examples of these natural textures.

Next, we aimed to use our proposed signatures to classify both image databases. To achieve this purpose we used linear discriminant

Fig. 5. Examples of each texture class considered in the VisTex database.

analysis (LDA), a classification method based on supervised learning [50,51]. Be $f_i(\mathbf{x})$ the density function of the population i, $i=1,2,\ldots,g$, the probability of misclassification is minimized according to the following discrimination rule: for a fixed observation $\mathbf{x}$, compute the density value $f_i(\mathbf{x})$ for each population i, $i=1,2,\ldots,g$, and classify the observation in the population k which presents the highest $f_i(\mathbf{x})$ value, i.e.

$$f_k(\mathbf{x}) = \arg\max\{f_i(\mathbf{x}), i = 1, 2, \ldots, g\},$$

with

$$f_i(\mathbf{x}) = -\tfrac{1}{2}\ln(|\Sigma_i|) - \tfrac{1}{2}(x-\mu_i)'\Sigma_i^{-1}(x-\mu_i)),$$

where μ and Σ_i are, respectively, the average vector and covariance matrix of the population i. More details about mathematical formulation of the discriminant function are presented in [52]. Moreover, *leave-one-out cross-validation* strategy was also performed over the LDA, whereby only one sample is used for validation while the others are used as a training set. The process of *training/validation* is repeated until all the samples were used for validation.

6. Evaluation

To evaluate the performance of the proposed fractal signatures, we designed a two-step evaluation. First, we evaluated each signature in order to determine the number of descriptors n that best characterizes the texture and its influence on the results of both databases. In the sequence, to provide a better evaluation of the proposed signatures, we performed a comparison with other color texture methods found in the literature. For this comparison, we considered the following methods: Gabor EEE [53,54], Histogram ratio features (HRF) [55], MultiLayer CCR [56], Linear prediction model [57,46] and an LBP+Haralick method [48]. A brief description of each method is presented as follows.

Gabor EEE measures a color texture by integrating over both the spatial dimension and the wavelength dimension. This method uses a linear transform from RGB to the Gaussian color model ($\tilde{E}$, $\tilde{E}_\lambda$ and $\tilde{E}_{\lambda\lambda}$). The measurements are obtained by applying a set of Gabor filters on each channel ($\tilde{E}$, $\tilde{E}_\lambda$ and $\tilde{E}_{\lambda\lambda}$). In our experiment, we used eight rotations and eight scales, with a lower frequency of 0.01 and an upper frequency of 0.4 (upper and lower frequencies are defined empirically). The setup of the individual parameters of each filter follows the mathematical model presented in [17]. The resulting feature vector presents the energy of 64 Gabor filters per color channel, what gives a total of 192 features.

Histogram ratio features (HRF) use the concept of co-occurrence in color histograms to extract meaningful information of a color texture. Basically, it computes the three-dimensional (3-D) color histogram of a given image. Then, it converts this histogram to a 1-D histogram and extracts ratio features as pairs of histogram bins combined with the corresponding count ratios. This method uses its own classification method, thus LDA method was not used to classify the samples due the number of descriptors is different for each texture.

MultiLayer CCR uses an approach similar to the one proposed for the $\mathrm{LBP}_{3\times3}$ operator [58]. At first, the method splits the original color image into a stack of binary images, each one representing a color of a predefined palette. This makes it possible to apply the CCR operator to each layer. Thus, each binary image is characterized by the probability of occurrence of rotation-invariant binary patterns, and the overall feature vector is obtained by concatenating the histograms computed for each layer. For this comparison, each image is represented by a total of 640 features. These features are obtained by using a palette of 64 colors and a 10 bins histograms for each palette entry.

The Linear prediction model (LPM) of [57] makes a quantitative comparison of auto spectra of luminance and combined chrominance channels of IHLS color space. The auto espectra is obtained using power spectrum estimator by the 2D multichannel non-symmetric half plane autoregressive (2D NSHP AR) model. To measure the similarity of two spectra the symmetric version of Kullback–Leibler divergence is used. A Knn classifier is constructed with this distance.

LBP + Haralick method [48] computes the vectorial LBP from color texture images which are coded in 28 different color spaces.

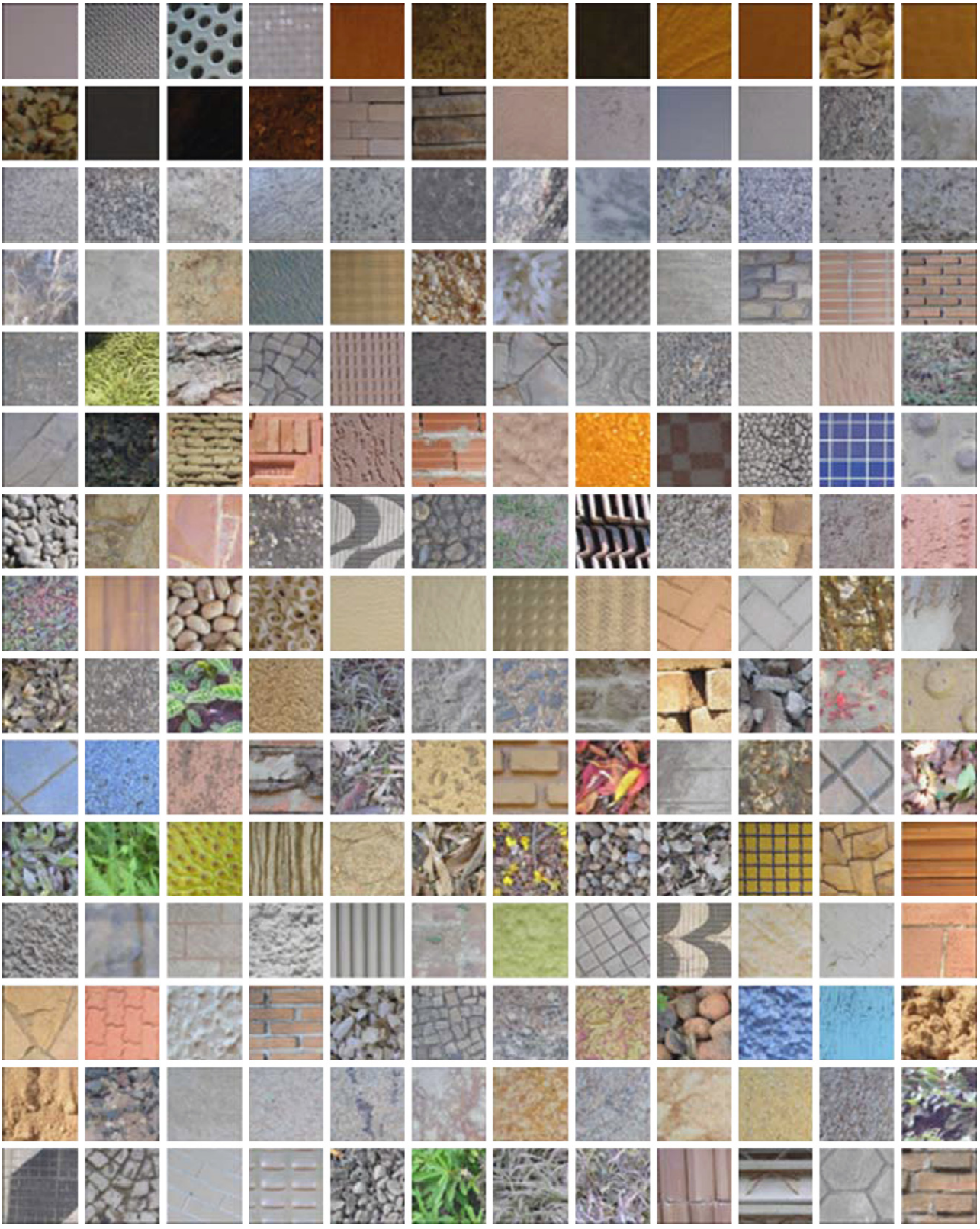

Fig. 6. Examples of each texture class considered in the Natural Textures database.

Then, the method computes Haralick features from the co-occurrence matrices computed from the resulting LBP images. The 10 most discriminate Haralick features are selected for texture classification.

Additionally, to evaluate the importance of color information in the results of our method, we computed the ψ signature from the gray scale version of both databases. Each RGB sample in the

databases was converted to gray scale by eliminating the hue and saturation information while retaining the luminance.

7. Results

We start by evaluating the proposed signatures according to the number of descriptors n used. Regarding the maximum dilation radius r, it is easy to see that too large values of r will increase the computational cost of the method: for a $N \times M$ pixels image with L gray levels, it is necessary to build a 3D volume of size $(N+2r) \times (M+2r) \times (L+2r+1)$; and too small values of r will significantly decrease the discrimination power of the resulting texture descriptor since a small value of r results in a log–log curve with few r_i points. In our experiments, we use $r=10$ as it achieves a good balance between computational cost and discrimination power of the resulting descriptor.

Figs. 7 and 8 present the results achieved in the VisTex and the USPTex texture databases, respectively. In general, the success rate yielded by each signature tends to increase as the number of descriptors n increases. We also note some oscillations during this process. These oscillations are a result of the proposed scheme to compute the signatures $\psi(n)$ and $\psi_{RGB}(n)$, where we select a total of n equidistant radius values from the log–log curve. A new signature $\psi(n+1)$ is different from its previous version $\psi(n)$ and it may not present the same discriminative properties present in the latter. In fact, this new signature could select radius values that present similar characteristics for different texture patterns, thus producing a small decrease in the success rate.

The best results are achieved when $n=33$ is considered. It is important to note that the results achieved by $\varphi(n)$ signature overcomes the ones from $\psi_{RGB}(n)$. An explanation for this behavior lies in the fact that the $\varphi(n)$ signature evaluates each color channel in an independent way. Thus, it provides more information about each color channel and as a consequence, about the whole image. As a result, we achieve a better texture discrimination. Otherwise, the $\psi_{RGB}(n)$ signature computes the color information of the three channels (R, G and B) in a single step, a sort of multi-spectral approach. Therefore, it uses only 33 descriptors to describe a color texture sample, while the $\varphi(n)$ signature uses 99 descriptors (33 descriptors per channel). This is the great advantage of this approach, but it is also its deficiency. Pixels at different color channels, but with the same intensity, are not as well represented in this approach as in the case where each color channel is independently analyzed. Thus, the description of a texture pattern with a strong correlation between its color channels may be unsuitable using the $\psi_{RGB}(n)$ signature.

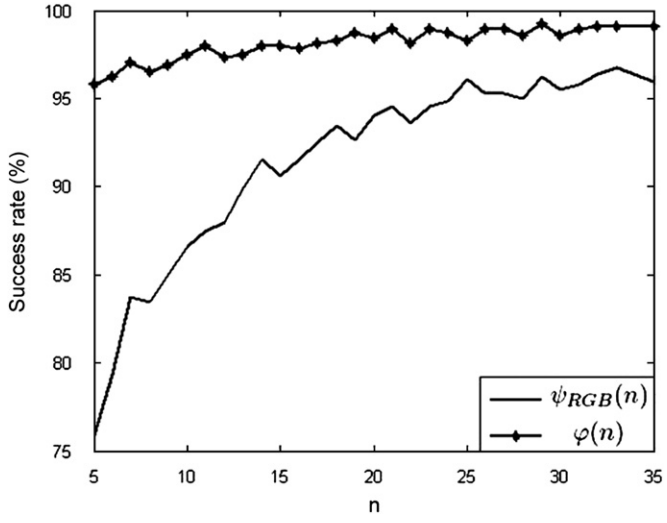

Fig. 7. Classification accuracy observed for different values of n in the VisTex database.

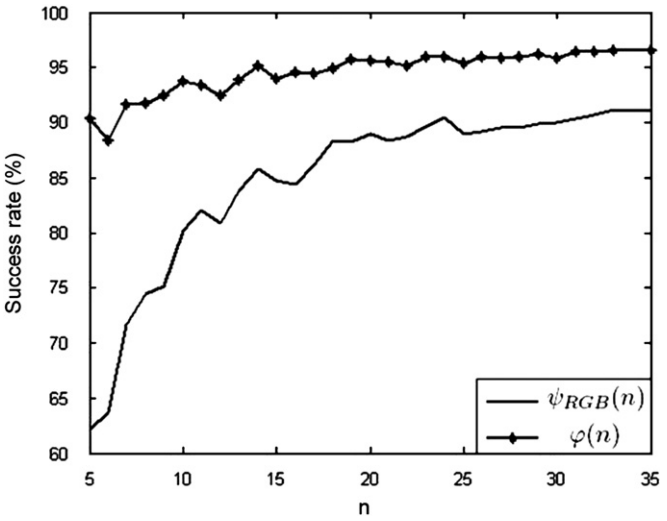

Fig. 8. Classification accuracy observed for different values of n in the USPText database.

Table 1
Results yielded by the proposed signatures and traditional texture analysis techniques.

Methods	No of descriptors	Success rate (%)	
		VisTex	Natural textures
φ signature	99	99.06	96.57
ψ_{RGB} signature	33	96.72	91.16
ψ_{Gray} signature [36]	33	93.28	81.11
Gabor EEE [53,54]	192	98.12	96.34
HRF [55]	–	66.56	48.61
MultiLayer CCR [56]	640	95.94	66.11
LPM [57]	–	95.48	85.92
LBP+Haralick [48]	10	93.12	81.53

Table 1 presents the results provided by the proposed signatures in comparison to other color-texture methods considered. Results clearly show that $\varphi(n)$ signature is more accurate in the classification of both image data sets as it presents the higher success rate. For success rate, we consider the percentage of images correctly classified in their respective classes. Its results are also impressive in terms of discrimination capability. The signature uses a reduced number of descriptors, i.e., half the number of descriptors of the Gabor EEE method, which was classified as the second best method in the experiment.

As expected, $\psi_{RGB}(n)$ signature presents an inferior performance in comparison to $\varphi(n)$ signature and Gabor EEE. As previously stated, this result is due to the reduced number of descriptors in this signature (in comparison to the $\varphi(n)$ signature) and its inability to deal with texture patterns presenting a strong correlation between its color channels. Still, the $\psi_{RGB}(n)$ signature is the one which presents the smallest number of descriptors at all. We must emphasize that the largest difference in the results achieved by the $\psi_{RGB}(n)$ and the Gabor EEE method is of 5.56%. However, our approach uses a sixth of the number of descriptors of the Gabor EEE method. Besides, our approach has the advantage of processing all color information in different color channels in a single step.

Another important characteristic of the proposed signatures is its robustness to the increase of the number of classes and samples in the database. From Vistex (40 classes) to the Natural Textures (180 classes) database, we note a drop of 2.49% and 5.63% in the $\varphi(n)$ and $\psi_{RGB}(n)$ signatures, respectively. The robustness of the method is comparable to the Gabor EEE method (drop of 1.78%). This characteristic is not present in other methods compared, such as the MultiLayer CCR, which presented a drop of almost 30% in its success rate as we change the database. Besides, MultiLayer CCR uses 640 descriptors to achieve a performance inferior than the one achieved by $\psi_{RGB}(n)$.

Between all methods, histogram ratio features (HRF) presented the lowest success rate in both databases. Its number of descriptors was not given as it depends on the color histogram of the image. Basically, the method considers only histogram bins with counts of more than 0.1% of the number of pixels in the given image.

As an additional experiment, we compared our color texture approaches with the $\psi_{Gray}(n)$ signature computed from the gray scale version [36] of both databases. This was performed to evaluate the importance of color information in our signature. Basically, we noticed a slight drop in the success rate at the time the color information is discarded in the Vistex database. However, the lack of color information contributes to decrease the robustness of the signature. $\psi_{Gray}(n)$ presents a more pronounced decrease in its success rate in comparison to $\psi_{RGB}(n)$ when it is used to classify the USPTex database. Since both signatures use the same number of descriptors, this is an indicative of the importance of color to discriminate the texture patterns. Still, the gray scale version of the proposed signature is more robust than Histogram ratio features (HRF) and MultiLayer CCR methods.

8. Conclusion

In this paper, we proposed a novel pattern recognition method based on complexity analysis. It was investigated how the color texture can be characterized and analyzed in terms of the fractal dimension. A signature which explores the details in the influence volume curve to perform a more precise texture characterization was defined. The potential of this signature was illustrated taking into account the independent dilation of R, G and B surfaces, and the dilation of the three channel in a single step, thus incorporating to the signature the information about the relationship between channels. The proposed signatures are capable of discriminating different classes with considerable quality, thus overcoming a traditional color texture analysis method, the Gabor EEE, in accuracy ($\varphi(n)$ signature) or number of descriptors (both signatures).

Acknowledgments

O.M.B. acknowledges support from CNPq (303746/2004-1 and 484474/2007-3). D.C. acknowledges support from FAPESP (2008/57313-2).

References

[1] Y.Q. Chen, M.S. Nixon, D.W. Thomas, Statistical geometrical features for texture classification, Pattern Recognition 28 (4) (1995) 537–552.
[2] F.M. Vilnrotter, R. Nevatia, K.E. Price, Structural analysis of natural textures, IEEE Transactions on Pattern Analysis and Machine Intelligence 8 (1) (1986) 76–89.
[3] R. Azencott, J.-P. Wang, L. Younes, Texture classification using windowed fourier filters, IEEE Transactions on Pattern Analysis and Machine Intelligence 19 (2) (1997) 148–153.
[4] A.K. Jain, F. Farrokhnia, Unsupervised texture segmentation using Gabor filters, Pattern Recognition 24 (12) (1991) 1167–1186.
[5] T. Randen, J.H. Husøy, Filtering for texture classification: a comparative study, IEEE Transactions on Pattern Analysis and Machine Intelligence 21 (4) (1999) 291–310.
[6] R.M. Haralick, Statistical and structural approaches to texture, Proceedings of IEEE 67 (5) (1979) 786–804.
[7] M. Tuceryan, A.K. Jain, Texture analysis, Handbook of Pattern Recognition and Computer Vision (1993) 235–276.
[8] J. Zhang, T. Tan, Brief review of invariant texture analysis methods, Pattern Recognition 35 (3) (2002) 735–747.
[9] L.J.V. Gool, P. Dewaele, A. Oosterlinck, Texture analysis anno 1983, Computer Vision, Graphics, and Image Processing 29 (3) (1985) 336–357.
[10] M. Petrou, P. García-Sevilla, Image Processing—Dealing with Texture, Wiley, 2006.
[11] M. Mirmehdi, X.H. Xie, J. Suri, Handbook of Texture Analysis, World Scientific, 2008.
[12] B. Julesz, Experiments in the visual perception of texture, Scientific American 232 (4) (1975) 34–43.
[13] V. Murino, C. Ottonello, S. Pagnan, Noisy texture classification: a higher-order statistics approach, Pattern Recognition 31 (4) (1998) 383–393.
[14] T.M. Caelli, B. Julesz, On perceptual analyzers underlying visual texture discrimination: part I, Biological Cybernetics 28 (1978) 167–176.
[15] J.M. Keller, S. Chen, R.M. Crownover, Texture description and segmentation through fractal geometry, Computer Vision, Graphics, and Image Processing 45 (2) (1989) 150–166.
[16] J. Daugman, C. Downing, Gabor wavelets for statistical pattern recognition, in: M.A. Arbib (Ed.), The Handbook of Brain Theory and Neural Networks, MIT Press, Cambridge, MA, 1995, pp. 414–419.
[17] B.S. Manjunath, W.-Y. Ma, Texture features for browsing and retrieval of image data, IEEE Transactions on Pattern Analysis and Machine Intelligence 18 (8) (1996) 837–842.
[18] R.K. Bajcsy, Computer identification of visual surfaces, Computer Graphics Image Processing 2 (1973) 118–130.
[19] M. Unser, Texture classification and segmentation using wavelet frames, IEEE Transactions on Image Processing 4 (11) (1995) 1549–1560.
[20] J.G. Daugman, Uncertainty relation for resolution in space, spatial frequency and orientation optimized by two-dimensional visual cortical filters, Journal of the Optical Society of America 2 (7) (1985) 1160–1169.
[21] J.E.W. Mayhew, J.P. Frisby, Texture discrimination and fourier analysis in human vision, Nature 275 (1978) 438–439.
[22] L.M. Kaplan, Extended fractal analysis for texture classification and segmentation, IEEE Transactions on Image Processing 8 (11) (1999) 1572–1585.
[23] H. Potlapalli, R.C. Luo, Fractal based classification of natural textures, in: Image Understanding Workshop, 1994, pp. II:1595–II:1606.
[24] M. Ivanovici, N. Richard, Fractal dimension of color fractal images, IEEE Transactions on Image Processing 20 (1) (2011) 227–235.
[25] A.P. Pentland, Fractal-based description of natural scenes, IEEE Transactions on Pattern Analysis and Machine Intelligence 6 (6) (1984) 661–674.
[26] S. Peleg, J. Naor, R.L. Hartley, D. Avnir, Multiple resolution texture analysis and classification, IEEE Transactions on Pattern Analysis and Machine Intelligence 6 (4) (1984) 518–523.
[27] J.J. Gangepain, C. Roques-Carmes, Fractal approach to two dimensional and three dimensional surface roughness, Wear 109 (1–4) (1986) 119–126.
[28] N. Sarkar, B.B. Chaudhuri, An efficient approach to estimate fractal dimension of textural images, Pattern Recognition 25 (9) (1992) 1035–1041.
[29] N. Sarkar, B.B. Chaudhuri, An efficient differential box-counting approach to compute fractal dimension of image, IEEE Transactions on Systems, Man and Cybernetics 24 (1994) 115–120.
[30] B.B. Chaudhuri, N. Sarkar, Texture segmentation using fractal dimension, IEEE Transactions on Pattern Analysis and Machine Intelligence 17 (1) (1995) 72–77.
[31] R. Rinaldo, A. Zakhor, Inverse and approximation problem for two-dimensional fractal sets, IEEE Transactions on Image Processing 3 (6) (1994) 802–820.
[32] A.R. Backes, O.M. Bruno, A new approach to estimate fractal dimension of texture images. in: ICISP, Lecture Notes in Computer Science, vol. 5099, Springer, 2008, pp. 136–143.
[33] J. Levy Vehel, P. Mignot, J.P. Berroir, Multifractals, texture, and image analysis, in: IEEE Computer Vision and Pattern Recognition or CVPR, 1992, pp. 661–664.
[34] A. Turiel, N. Parga, The multifractal structure of contrast changes in natural images: from sharp edges to textures, Neural Computation 12 (4) (2000) 763–793.
[35] R. de O. Plotze, J.G. Pádua, M. Falvo, L.C.B., G.C.X. Oliveira, M.L.C. Vieira, O.M. Bruno, Leaf shape analysis by the multiscale minkowski fractal dimension, a new morphometric method: a study in passiflora l. (passifloraceae), Canadian Journal of Botany-Revue Canadienne de Botanique 83(3) (2005) 287–301.
[36] A.R. Backes, D. Casanova, O.M. Bruno, Plant leaf identification based on volumetric fractal dimension, International Journal of Pattern Recognition and Artificial Intelligence 23 (6) (2009) 1145–1160.
[37] A.C. She, T.S. Huang, Segmentation of road scenes using color and fractal-based texture classification, in: ICIP (3), 1994, pp. 1026–1030.
[38] N. Asada, T. Matsuyama, Color image analysis by varying camera aperture, in: International Conference on Pattern Recognition, 1992, pp. I:466–I:469.

[39] G. Neil, K.M. Curtis, Shape recognition using fractal geometry, Pattern Recognition 30 (12) (1997) 1957–1969.
[40] B. Mandelbrot, The Fractal Geometry of Nature. Freeman & Co.
[41] C. Tricot, Curves and Fractal Dimension, Springer-Verlag, 1995.
[42] O.M. Bruno, L. da Fontoura Costa, A parallel implementation of exact Euclidean distance transform based on exact dilations, Microprocessors and Microsystems 28 (3) (2004) 107–113.
[43] T. Saito, J.-I. Toriwaki, New algorithms for Euclidean distance transformation of an *n*-dimensional digitized picture with applications, Pattern Recognition 27 (11) (1994) 1551–1565. 〈http://dx.doi.org/10.1016/0031-3203(94)90133-3〉.
[44] Å. Björck, Numerical Methods for Least Squares Problems, SIAM, Philadelphia, 1996.
[45] T. Maenpaa, M. Pietikainen, Classification with color and texture: jointly or separately? Pattern Recognition 37 (8) (2004) 1629–1640.
[46] I.-U.-H. Qazi, O. Alata, J.-C. Burie, A. Moussa, C. Fernandez-Maloigne, Choice of a pertinent color space for color texture characterization using parametric spectral analysis, Pattern Recognition 44 (1) (2011) 16–31.
[47] P. Denis, P. Carre, C.F. Maloigne, Spatial and spectral quaternionic approaches for colour images, Computer Vision and Image Understanding 107 (1–2) (2007) 74–87.
[48] A. Porebski, N. Vandenbroucke, L. Macaire, Haralick feature extraction from LBP images for color texture classification, in: Image Processing Theory, Tools and Applications, 2008, pp. 1–8. URL: 〈http://dx.doi.org/10.1109/IPTA.2008.4743780〉.
[49] Vision texture database (2009). URL: 〈http://vismod.media.mit.edu/vismod/imagery/VisionTexture/vistex.html〉.
[50] J.F. Hair, R.E. Anderson, R.L. Tatham, W.C. Black, Multivariate Data Analysis, Prentice Hall College Div, 1998 (Peter's Book).
[51] K. Fukunaga, Introduction to Statistical Pattern Recognition, 2nd ed., Academic Press, Boston, MA, 1990.
[52] R. Johnson, D. Wichern, Applied Multivariate Statistical Analysis, Prentice-Hall, Englewood Cliffs, NJ, 1982.
[53] M.A. Hoang, J.M. Geusebroek, Measurement of color texture, in: Workshop on Texture Analysis in Machine Vision, 2002, pp. 73–76.
[54] M.A. Hoang, J.-M. Geusebroek, A.W.M. Smeulders, Color texture measurement and segmentation, Signal Processing 85 (2) (2005) 265–275.
[55] G. Paschos, M. Petrou, Histogram ratio features for color texture classification, Pattern Recognition Letters 24 (1–3) (2003) 309–314.
[56] F. Bianconi, A. Fernandez, E. Gonzalez, D. Caride, A. Calvino, Rotation-invariant colour texture classification through multilayer CCR, Pattern Recognition Letters 30 (8) (2009) 765–773.
[57] I.-U.-H. Qazi, O. Alata, J.-C. Burie, C. Fernandez-Maloigne, Color spectral analysis for spatial structure characterization of textures in IHLS color space, Pattern Recognition 43 (3) (2010) 663–675.
[58] T. Ojala, M. Pietikainen, T. Maenpaa, Multiresolution gray-scale and rotation invariant texture classification with local binary patterns, IEEE Transactions on Pattern Analysis and Machine Intelligence 24 (7) (2002) 971–987.

André Ricardo Backes is a professor at the College of Computing at the Federal University of Uberlândia in Brazil. He received his B.Sc. (2003), M.Sc. (2006), and Ph.D. (2010) in Computer Science at the University of S. Paulo. His fields of interest include Computer Vision, Image Analysis and Pattern Recognition.

Dalcimar Casanova has received his Master degree in Computer Science at ICMC-USP and is currently Ph.D. student in Computational Physics at IFSC-USP. His fields of interest include computer vision, biological computing and machine learning.

Odemir Martinez Bruno is an associate professor at the Institute of Physics of S. Carlos at the University of S. Paulo in Brazil. He received his B.Sc. in Computer Science in 1992, from the Piracicaba Engineering College (Brazil), his M.Sc. in Applied Physics (1995) and his Ph.D. in Computational Physics (2000) at the University of S. Paulo (Brazil). His fields of interest include Computer Vision, Image Analysis, Computational Physics, Pattern Recognition and Bioinformatics. He is an author of many papers (journal and proceedings) and several book chapters, co-author of two books (Optical and Physiology of Vision: a multidisciplinary approach (Portuguese only) and Internet programming with PHP (Portuguese only)) and an inventor of five patents.